Shock-wave structure based on the Navier-Stokes-Fourier equations

F. J. Uribe* and R. M. Velasco†
Department of Physics, Universidad Autónoma Metropolitana–Iztapalapa, Apartado Postal 55–534, C.P. 09340, México, D.F., México

(Received 8 February 2018; published 30 April 2018)

We use the Navier-Stokes-Fourier constitutive equations to study plane shock waves in dilute gases. It is shown that the experimental information on the normalized density profiles can be fit by using the so-called soft sphere model, in which the viscosity and thermal conductivity are proportional to a power of the temperature.

DOI: 10.1103/PhysRevE.97.043117

I. INTRODUCTION

The dynamical theory of fluids has been studied for a long time and the field has broadened enormously its application to several subjects [1]. Despite all the successes coming from them, some problems are not completely solved, such as an accurate description of the shock-wave structure in simple fluids. There are at least four main approaches to study such a problem. Let us first briefly describe how the Boltzmann equation for simple fluids and its methods of solution are used to deal with the shock-wave profiles. In a broad way we group the papers around two branches of development. The branch based on normal solutions is exemplified by the Chapman-Enskog method to obtain an approximation for the distribution function which solves the Boltzmann equation [2] (or the Bhatnagar-Gross-Krook, BGK model [3]), in which a perturbation expansion in terms of the Knudsen number is done. It is well known that this methodology drives the Euler constitutive equations to the lowest order, then the Navier-Stokes-Fourier (NSF) constitutive set of equations is obtained, whose application to the shock-wave problem has a long history [4–7]. They contain the dissipative effects caused by the transport processes in the system, represented mainly by the viscosity and the thermal conductivity. Such transport coefficients depend on the interaction potential between particles in the gas, and the search for a proper potential has provided hard work for several years. The Burnett equations [8], which can be obtained with the Chapman-Enskog method to second order in the Knudsen number [2], and the method of stretched fields or Maxwellian iteration [9], are well-known attempts to extend the NSF hydrodynamics that, besides the NSF constitutive equations, rely on equations of state and the conservation equations. Its derivations, limitations, modifications, renormalizations, regularizations, and generalizations are discussed in the literature [10–23]. However, we have the moment solution branch [23–37], where the Maxwell-Cattaneo equations may be considered as a precursor theory for this branch that is based on an expansion of the distribution function in terms of a complete set of functions (usually Hermite tensor polynomials). The main problem being the closure hypothesis needed to cut the expansion. However, the NSF constitutive equations have been obtained from this method, which provides a way to extend them. It should be mentioned that both branches do not exclude each other, in a certain way they may be considered as complementary lanes to solve the kinetic equation. Also, there have been several attempts to generalize the NSF hydrodynamic equations or methods that have been useful for shock waves, which are neither necessarily linked to the Boltzmann equation solutions nor restricted to dilute gases. Some examples for these approaches are the Maxwellian iteration method or the method of stretched fields [9,16,18,33] and the Mott-Smith method and its variants [38–41]: the two or multitemperature theories [42–49], the two-velocity theory [50–53], the finite-scale equations [54,55] for compressible flows, the two-fluids theory [56], among others.

Second, the NSF constitutive equations have been modified phenomenologically through some considerations about their structure and the temperature dependence in the transport coefficients [43]. We will insist on that in this work. As a third approach we consider the numerical methods, such as the direct simulation Monte Carlo (DSMC) [57,58], the molecular dynamics calculations (MD) [11,59], and the lattice Boltzmann gas [60–62]. The results coming from them can be considered as experimental data to describe the shock-wave behavior to compare with the calculations based on the kinetic or the phenomenological theories. Finally, the experimental data obtained directly in shock tubes provide us with elements to decide about the robustness of the underlying models [63–66]. It is not our purpose to give a detailed account of such attempts, instead we bring back our attention to the NSF constitutive equations. In fact, we will show that it is possible to fit the experimental information concerning the normalized density profiles for shock waves using the NSF constitutive equations, provided that we include a modification in the viscosity and the thermal conductivity to enhance their effects. In addition, we use the ideal gas law, equipartition of energy (we assume that both hold locally along the shock wave), and the conservation equations.

The structure of this work is as follows. After this Introduction, we study the NSF constitutive equations for the case of a plane shock wave and derive the corresponding NSF

*paco@xanum.uam.mx
†rmvb@xanum.uam.mx

hydrodynamic model used here. Then, we compare the numerical solutions obtained with the experimental information and the direct simulation Monte Carlo method. We give some remarks in the concluding section.

II. THE NAVIER-STOKES-FOURIER EQUATIONS

Let us begin with the conservation equations for mass, momentum, and energy fluxes valid for a plane one-dimensional shock wave [4], namely,

$$\rho(x)\,u(x) = C_1, \tag{1a}$$

$$P_{xx}(x) + \rho(x)\,u(x)^2 = C_2, \tag{1b}$$

$$\rho(x)\,u(x)\left[e(x) + \frac{P_{xx}(x)}{\rho(x)} + \frac{u(x)^2}{2}\right] + q(x) = C_3, \tag{1c}$$

where $\rho(x)$ is the mass density, $u(x)$ is the hydrodynamic velocity, $P_{xx}(x)$ is the xx component of the pressure tensor, $e(x)$ is the specific internal energy, $q(x)$ is the heat flux, and the quantities C_1, C_2, and C_3 are constants. The previous conservation equations must be supplemented with the equation of state and the internal energy for a dilute gas, which will be assumed as an ideal one,

$$p(x) = \rho(x)\,\frac{k_B\,T(x)}{m}, \quad e(x) = \frac{3\,k_B\,T(x)}{2\,m}, \tag{2}$$

where k_B is the Boltzmann constant and m is the mass. Besides, the constitutive equations for the xx component in the pressure tensor and the heat flux are taken from the usual Navier-Newton and Fourier empirical laws; they read as

$$P_{xx}(x) = p(x) - \frac{4}{3}\,\eta[T(x)]\,\frac{du(x)}{dx}, \tag{3}$$

$$q(x) = -\kappa[T(x)]\,\frac{dT(x)}{dx}, \tag{4}$$

where η is the shear viscosity and κ is the thermal conductivity. Both depend on the temperature. The constants written above are determined by the Rankine-Hugoniot jump conditions,

$$\rho_0\,u_0 = \rho_1\,u_1 = C_1, \tag{5}$$

$$\rho_0\frac{k_B\,T_0}{m} + \rho_0\,u_0^2 = \rho_1\frac{k_B\,T_1}{m} + \rho_1\,u_1^2 = C_2, \tag{6}$$

$$\frac{5\,k_B T_0}{2\,m} + \frac{u_0^2}{2} = \frac{5\,k_B T_1}{2\,m} + \frac{u_1^2}{2} = C_3/C_1, \tag{7}$$

where subscripts 0 and 1 in the temperature and the velocity refer to the cold (where the flow is supersonic) and hot (where the flow is subsonic) parts of the shock, respectively. The differential equations to be solved result when the constitutive relations are substituted in the conservation equations, then the conservation of mass is used to express the mass density in terms of the velocity. Hence, the conservation equations of momentum and energy, Eqs. (1b) and (1c), can be written as follows:

$$C_1\,\frac{k_B\,T}{m\,u} - \frac{4}{3}\,\eta(T)\,\frac{du}{dx} + C_1\,u = C_2, \tag{8a}$$

$$\frac{5\,k_B\,T}{2\,m} - \frac{4}{3}\frac{\eta(T)}{C_1}\,u\,\frac{du}{dx} + \frac{u^2}{2} - \frac{\kappa(T)}{C_1}\,\frac{dT}{dx} = C_3/C_1. \tag{8b}$$

It is convenient to use dimensionless variables defined as follows:

$$v(s) \equiv u(x)/u_0, \quad T^*(s) \equiv k_B\,T(x)/m\,u_0^2,$$
$$\eta^*[T^*(s)] \equiv \eta[T(x)]/\eta_0, \quad \kappa^*[T^*(s)] \equiv \kappa[T(x)]/\kappa_0, \tag{9}$$

where η_0 and κ_0 are the viscosity and thermal conductivity at T_0, respectively, and the variable

$$s \equiv x/\lambda \tag{10}$$

is a dimensionless distance whose specific definition, the value of the length λ, is given below. In terms of the previous reduced variables, Eqs. (8) take the form

$$\frac{T^*}{v} - \eta^*(T^*)\left(\frac{4\,\eta_0}{3\,\lambda\,C_1}\right)\frac{dv}{ds} + v = 1 + T_0^*, \tag{11a}$$

$$\frac{5}{2}T^* - \eta^*(T^*)v\left(\frac{4\,\eta_0}{3\,\lambda\,C_1}\right)\frac{dv}{ds} + \frac{v^2}{2} - \kappa^*(T^*) \times \left(\frac{\kappa_0\,m}{k_B\lambda\,C_1}\right)\frac{dT^*}{ds} = \frac{1}{2} + \frac{5}{2}\,T_0^*, \tag{11b}$$

where we recall that the viscosity and thermal conductivity depend on the temperature, so $\eta^*(T^*)$, $\kappa^*(T^*)$. In the literature, the value for λ has been taken in several ways, one election which is used to report the experimental measurements is given in Refs. [63–66],

$$\lambda_A \equiv \frac{16}{5}\left(\frac{5}{3}\,\frac{1}{2\,\pi}\right)^{1/2}\frac{\eta_0}{\rho_0\,a_0}, \tag{12}$$

where a_0 is the velocity of sound at T_0. For simplicity, we will use for λ the value

$$\lambda = \frac{4}{3}\,\frac{\eta_0}{C_1} = \frac{4}{3}\,\frac{\eta_0}{\rho_0\,u_0}, \tag{13}$$

so that Eq. (11a) takes a simple form. For a given reference system and a value of the position x, we call $s_A \equiv x/\lambda_A$ and $s \equiv x/\lambda$, then the solutions using s_A or s are related as

$$v(s_A) = v(s), \quad T^*(s_A) = T^*(s), \tag{14}$$

with

$$\lambda = \frac{5}{12}\,\sqrt{2\,\pi\,T_0^*}\,\lambda_A. \tag{15}$$

Using Eq. (13), we are lead to the following explicit dynamical system that can be obtained from Eqs. (11):

$$\frac{dv}{ds} = \frac{v^2 - (1 + T_0^*)\,v + T^*}{v\,\eta^*(T^*)}, \tag{16a}$$

$$\frac{dT^*}{ds} = \frac{2\,k_B\,\eta_0}{3\,m\,\kappa_0}\;\frac{-v^2 + 2\,(1 + T_0^*)\,v + 3\,T^* - (1 + 5\,T_0^*)}{\kappa^*(T^*)}. \tag{16b}$$

These equations must be solved by taking into account the Rankine-Hugoniot jump conditions that in terms of the reduced variables introduced before, see Eqs. (5)–(7), give us the following values for v and T^* written in terms of the Mach

number at up-flow $M^2 = \frac{3}{5T_0^*}$:

$$\text{Up-flow coordinates:} \quad v_0 = 1, \quad T_0^* = \frac{3}{5M^2}, \tag{17}$$

$$\text{Down-flow coordinates:} \quad v_1 = \frac{3+M^2}{4M^2} = \frac{1}{4} + \frac{T_0^*}{4},$$

$$T_1^* = \frac{3\,(-3+14M^2+5M^4)}{80M^4} = \frac{3}{16} + \frac{7}{8}\,T_0^* - \frac{5}{16}\,T_0^{*2}. \tag{18}$$

The problem is to find a solution curve to the dynamical system given by Eqs. (16) that joins the two critical, or equilibrium, points (down-flow and up-flow). In the mathematical parlance, such a curve is called a heteroclinic trajectory or heteroclinic orbit. For the Navier-Stokes an existence theorem for such shock-wave solution (the heteroclinic trajectory) is known as well as a methodology to find an approximation to it [6]. To find an approximation, it is convenient to know the nature of the critical points, for the Navier-Stokes equations up-flow is an unstable node while down-flow is a saddle. Then, one starts near down-flow and integrates the dynamical system by decreasing x ("the integration is performed in the negative sense"), such a procedure gives an approximation for the heteroclinic trajectory. In practice, the initial conditions, denoted by (v_i, T_i^*), are obtained by perturbing down-flow; we used $(v_i, T_i^*) = (v_1 + 10^{-10}, T_1^*)$ [43].

While there has been several works dealing with the Navier-Stokes equations for shock waves, we would like to bring to the fore one aspect that as far we know has not been considered in the literature. It is possible to fit the experimental normalized density profiles using the Navier-Stokes equations by assuming that the viscosity is proportional to a power of the temperature (the soft sphere model),

$$\eta \sim T^\sigma, \tag{19}$$

where the fitting parameter is provided by the viscosity-temperature index σ.

For simplicity, we will use the first Sonine approximation [2], which is supported by experimental values and the corresponding states principle [35],

$$\frac{m\,\kappa}{k_B\,\eta} = \frac{15}{4} \Rightarrow \kappa^* = \eta^* = \left(\frac{T^*}{T_0^*}\right)^\sigma. \tag{20}$$

Now the equations to be solved are written as follows:

$$\frac{dv}{ds} = \frac{v^2 - (1+T_0^*)\,v + T^*}{v\,T^{*\sigma}}\,T_0^{*\sigma}, \tag{21a}$$

$$\frac{dT^*}{ds} = \frac{8}{45}\,\frac{-v^2 + 2\,(1+T_0^*)\,v + 3\,T^* - (1+5\,T_0^*)}{T^{*\sigma}}\,T_0^{*\sigma}. \tag{21b}$$

Solutions to the previous differential equations that can be expressed in terms of elementary functions are not known, and there probably are none, but a proof is lacking. Therefore, numerical methods are used to solve the dynamical system. However, an implicit solution to Eqs. (16) was found by Becker in 1922 for constant transport coefficients and a Prandtl number of value 3/4. The details, analysis, and generalizations can be found in the literature [5,7]. In our case, Eq. (20) gives a Prandtl number of value 2/3 that gives a better agreement with the experimental information for dilute gases. Taylor gave another (implicit) solution for the case when either the viscosity or the thermal conductivity is zero [4], and there is a well-known approximate explicit solution for weak shocks that can be expressed in terms of the hyperbolic tangent and is not restricted to dilute gases [1]. For weak shocks in gases, a similar solution, written in terms of the hyperbolic tangent, was found by Taylor [4] and has been discussed in the existence theorem for shock profile solutions to the Boltzmann equation by Caflisch and Nicolaenko [67]; solutions to the Boltzmann equation for very strong shocks of hard spheres have also been discussed in the literature [68].

From Eqs. (21), we notice that the derivative of the reduced temperature with respect to the reduced velocity is

$$\frac{dT^*}{dv} = \frac{8}{45}\,\frac{v\,[-v^2 + 2\,(1+T_0^*)\,v + 3\,T^* - (1+5\,T_0^*)]}{v^2 - (1+T_0^*)\,v + T^*}, \tag{22}$$

from which we conclude that the solution curves (orbits) are locally independent of the viscosity-temperature index (σ).

In terms of the Mach number and using Alsmeyer's mean free path (λ_A), the equations to be solved for the soft sphere model are

$$\frac{dv}{ds_A} = \frac{2}{25}\sqrt{\frac{30}{\pi}}\,\frac{5\,v^2M^2 - v\,(5\,M^2+3) + 5\,T^*\,M^2}{M\eta^*\,v}, \tag{23a}$$

$$\frac{dT^*}{ds_A} = -\frac{16}{1125}\sqrt{\frac{30}{\pi}} \times \frac{5\,v^2M^2 - 2\,v(5\,M^2+3) - 15\,T^*\,M^2 + 5\,(M^2+3)}{M\,\eta^*}, \tag{23b}$$

where

$$\eta^* = \left(\frac{5\,M^2\,T^*}{3}\right)^\sigma. \tag{24}$$

Given the initial conditions mentioned previously for v and T^*, the initial value of s_A (or s) is taken in such a way that the normalized density, ρ_n, has the value 1/2 at the origin. It should be noticed that Eqs. (23) are translational invariant, a fact that can be seen in the following way. Let c be any constant, if we define $\hat{v}(s) = v(s+c)$ and $\tau(s) = T^*(s+c)$ or $\hat{v}(s_A) = v(s_A+c)$ and $\tau(s_A) = T^*(s_A+c)$, then Eqs. (21) and (23) retain the same form in terms of $\hat{v}$ and τ. This means that both sets of differential equations are translational invariant, it is a common practice to fix the election of the origin of the coordinate system ($s=0$, $s_A=0$, $x=0$), so that the normalized density profile, defined by Eq. (25), has the value 1/2 at the origin, and we will use such a convention.

III. COMPARISON WITH EXPERIMENTS AND THE DSMC METHOD

There is a fair amount of information on the shock-wave problem and here we consider experiments that provide the normalized density profiles, and quantities derived from it such as the reciprocal shock thickness and the asymmetry of the

density profiles. In addition, if simulations are available, it is possible to obtain information on the temperature profiles and the shock-wave behavior in the plane v-T^*. The definitions and relevant information for these quantities as well as comparisons with experiments and simulations are given below. Since Eqs. (21) for v and T^* are coupled, it is possible to have good normalized density profiles but not necessarily the temperature profiles will automatically be good. Therefore, we consider necessary to give a detailed account of several features that have been considered in the literature to discuss properly the shock-wave problem.

The experimental information is given for the normalized density profile $\rho(s_A)$ [63–66]. It is defined as

$$\rho_n(s_A) = \frac{\rho(s_A) - \rho_0}{\rho_1 - \rho_0}, \tag{25}$$

where $\rho_n(s_A)$ is called as the normalized density profile, ρ_0 and ρ_1 are its values at the cold and hot parts of the shock, respectively. Several works dealing with the NSF constitutive equations to study shock waves assume a certain value for the viscosity-temperature index σ, though there is not a general agreement about its precise value. For example, the experimental comparison for the normalized density profile using the NSF constitutive equations done by Schmidt [63] and Alsmeyer [65] take $\sigma = 0.68$ or $\sigma = 0.72$. It is also possible to use the corresponding states principle [35], which gives information of the viscosity, to solve Eqs. (21) without assuming the specific temperature dependence given by the soft sphere model, the results of this procedure give practically the same normalized density profiles as the soft sphere model with $\sigma = 0.72$ for Mach numbers in the range; $M \in [1,2]$ [35]. The DSMC also uses a viscosity proportional to a temperature power to study shock waves for Argon, the recommended value is $\sigma = 0.81$ [57,58]. However, Greenshields and Reese [51] argued that for Mach numbers about 10 the value $\sigma = 0.76$ gives a better fit to available information for the viscosity; they actually suggested to use the viscosity-temperature index as an adjustable parameter to fit the experimental values of the viscosity, and in this work we will use it to fit the experimental normalized density profiles.

The DSMC computations reported here use the variable soft sphere (VSS) interaction model, which in addition to the variable molecular diameter $d \propto c_r^{-\vartheta}$, considers that the deflection angle (χ) in the binary collision is given by

$$\chi = 2\cos^{-1}(b/d)^{1/\alpha}, \tag{26}$$

where c_r is the relative velocity in a binary elastic collision, $\vartheta = \sigma - 1/2$ with σ the viscosity-temperature index, and b is the impact parameter. So that two parameters characterize the VSS interaction model. The normalized density profiles provided by Bird's DSMC are given in terms of the mean free path defined by him (λ_B) [57]:

$$\lambda_B = \frac{4\alpha(5-2\sigma)(7-2\sigma)\beta_0\eta_0}{5\sqrt{\pi}(\alpha+1)(\alpha+2)\rho_0}, \quad \text{where} \quad \beta_0 = \sqrt{\frac{m}{2k_BT_0}}. \tag{27}$$

The results shown in Fig. 1 come from the comparison between the normalized density as calculated with Eqs. (21), or Eqs. (23), with the soft sphere model and the experimental values for some Mach numbers. The DSMC computations are also included for different values of the viscosity-temperature index; in general, the agreement shown is very good. In all the normalized density profiles plots, up-flow is at the far left side of them. A more detailed quantitative information is provided in Table I for Argon at $M = 8$ and different values of the temperature-viscosity index. One infers that the use of $\sigma = 0.9$ provides a significant improvement with respect to the value $\sigma = 0.72$, but the behavior of the solution with $\sigma = 0.9$ is not accurate, when compared to the experimental data, near up-flow (see $s_A = -6.0, -5.0, -4.0$ in Table I).

Also, apart from the comparisons between the normalized density profiles, there are other characteristics that have been considered, namely,

(i) Reciprocal shock thickness (inverse density thickness). It is defined by [69]

$$\delta^{-1} = \frac{1}{\rho_1 - \rho_0}\max\{|\rho'(x)|\}, \tag{28}$$

where the prime denotes the derivative of the density profile and max refers to its maximum value within the profile. We obtain that

$$\delta^{-1} = \frac{\max\{|d\rho_n/ds_A|\}}{\lambda_A} = \frac{1}{\lambda_A}\frac{12}{5\sqrt{2\pi T_0^*}}\frac{\max\{|d\rho^*/ds|\}}{(\rho_1^* - 1)}, \tag{29}$$

with $\rho^*(s) = \rho(x)/\rho_0 = 1/v(s)$.

(ii) Asymmetry of the density profiles (density asymmetry quotient), Q [65]. Defined as $Q = \lim_{s\to\infty}\overline{Q}(s)$, with

$$\overline{Q} = \frac{\int_{-s}^{0}\rho_n(s')ds'}{\int_0^s[1-\rho_n(s')]ds'}. \tag{30}$$

It should be mentioned that both properties in the shock structure are in fact a different measure of the shock structure. The inverse shock thickness represents a local one, whereas the asymmetry factor shows a kind of global measure.

The results of our calculations for the two previous quantities are given in Table II. From the values given it follows that the approach used here not only provides very good profiles but also the experimental values for the reciprocal shock thickness as well as the asymmetry factor are reproduced. Certainly, the following comments must be taken into account. First, the experimental data have dispersion as all experiments have. Second, the agreement shown is good and it is done with just one parameter, though both properties are related with the density profile. At this point we recall the comment made by Schmidt [63]: "Shock-wave thickness fails to give sufficiently detailed information about structure; calculated and measured profiles may differ considerably, but the thickness can be the same." However, there is a loose point in the previous remark: The normalized density profiles obtained with Eqs. (21) are accurate when compared to the experiments, therefore agreement with both the inverse shock thickness and the asymmetry of the density profiles is to be expected, though apparently it is not the case. As an example, take the case for $M = 8$ where the experimental shock thickness and the one calculated with Eqs. (21) are nearly the same, see Table II, but the asymmetry factor is not. For $M = 8$, the experimental value reported by Schmidt [63] is $Q_S \approx 1.15$, while Eqs. (21) with $\sigma = 0.9$ give $Q(\sigma = 0.9) = 1.26$, whereas $Q(\sigma = 0.68) \approx$

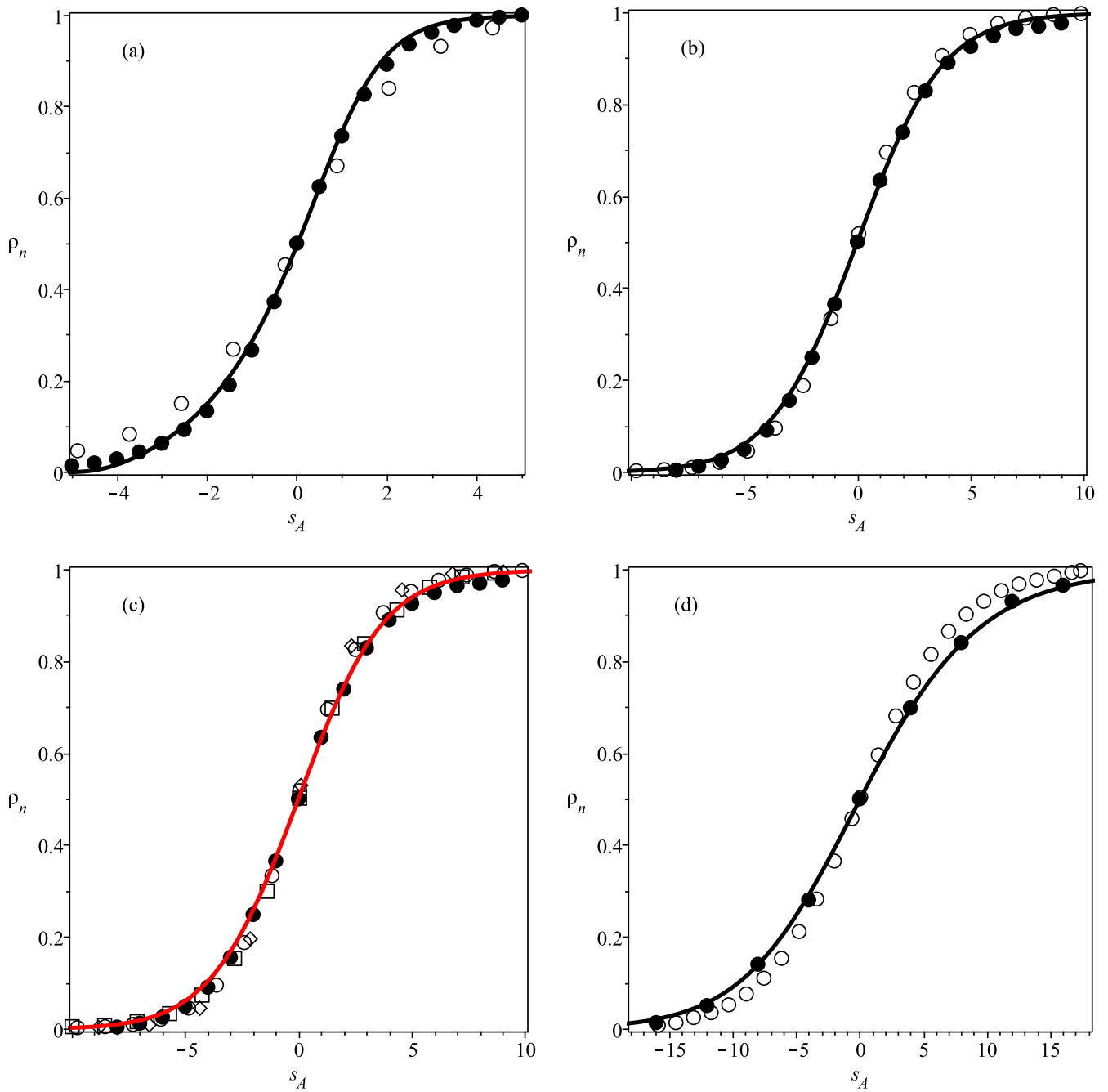

FIG. 1. Normalized density profiles vs the reduced distance, ρ_n vs s_A, for Argon at different Mach numbers. (a) M = 8. Solid circles: experiments from Steinhilper [64]; open circles: DSMC for $\sigma = 0.81$ and $\alpha^{-1} = 0.6015$; solid line: solution to Eqs. (23) for $\sigma = 0.9$. (b) M = 1.55. Solid circles: experiments from Alsmeyer [65]; open circles: DSMC for $\sigma = 0.81$ and $\alpha^{-1} = 0.6525$; solid line: solution to Eqs. (23) for $\sigma = 1.6$. (c) M = 1.55. Solid circles: experiments from Alsmeyer [65]; open circles: DSMC for $\sigma = 0.81$ and $\alpha^{-1} = 0.6525$, diamonds: DSMC for σ (Maxwell model) and $\alpha^{-1} = 0.6525$, boxes: DSMC for $\sigma = 0.0$ (constant transport coefficients) and $\alpha^{-1} = 0.6525$. The DSMC results using $\alpha^{-1} = 0.6015$ give practically the same output when $\alpha^{-1} = 0.6525$ is used. (d) M = 1.2. Solid circles: experiments from Garen *et al.* [66]; open circles: DSMC for $\sigma = 0.81$ and $\alpha^{-1} = 0.6015$; solid line: solution to Eqs. (23) for $\sigma = 3$.

1.45 [63], certainly the first value gives a better agreement with the experimental one, but it seems that there is room for improvement. Other comparisons of the asymmetry of the density profiles for different theories and the experiments are available [51,70].

We now discuss additional information on the shock-wave structure that can be obtained with the use of simulations. As far as we know, there is not experimental information on the temperature profiles for shock waves, but we can use the DSMC calculations to calculate them and show that Eqs. (21) with the viscosity-temperature index quoted are not consistent with DSMC results for high Mach numbers ($M = 8$). To show this we consider the orbits, that is, the solution curve in the v-T^* plane for two different Mach numbers. In Fig. 2 a comparison

TABLE I. Normalized density profiles vs reduced distance, ρ_n vs s_A, for Argon at $M = 8$. The experimental values are taken from the work by Steinhilper [64]. Theory refers to the numerical solution of Eqs. (21) for different values of the temperature-viscosity index, and in parentheses we provide the numerical solution to Eqs. (23).

Reduced distance	Experiment	Theory ($\sigma = 0.90$)	Theory ($\sigma = 0.72$)	Theory ($\sigma = 1.05$)
s_A	ρ_n	ρ_n	ρ_n	ρ_n
7.0	1.009	1.000 (1.001)	1.000 (1.019)	0.997 (0.997)
6.0	1.006	1.000 (1.000)	1.000 (1.007)	0.993 (0.992)
5.0	1.000	0.999 (0.998)	1.000 (1.002)	0.982 (0.982)
4.0	0.989	0.994 (0.994)	1.000 (1.001)	0.958 (0.957)
3.0	0.962	0.977 (0.977)	0.999 (0.999)	0.905 (0.904)
2.0	0.892	0.914 (0.914)	0.986 (0.987)	0.807 (0.806)
1.0	0.735	0.748 (0.747)	0.879 (0.879)	0.662 (0.662)
0.0	0.500	0.500 (0.500)	0.500 (0.500)	0.500 (0.500)
−1.0	0.266	0.289 (0.288)	0.191 (0.190)	0.354 (0.354)
−2.0	0.133	0.151 (0.150)	0.056 (0.055)	0.239 (0.239)
−3.0	0.062	0.066 (0.066)	0.006 (0.006)	0.153 (0.152)
−4.0	0.028	0.017 (0.017)	0.000 (0.000)	0.089 (0.088)
−5.0	0.013	0.001 (0.001)	0.000 (0.000)	0.042 (0.041)
−6.0	0.006	0.000 (0.000)	0.000 (0.000)	0.010 (0.010)

for $M = 1.2$ and $M = 8$ is shown. For $M = 1.2$ there is very good agreement between the orbits but there is a noticeable difference of the orbits given by the NSF equations and those obtained from the DSMC method. Therefore, Eqs. (21) do not provide agreement with the DSMC method for high Mach numbers when the orbits are considered. Another difference is that the DSMC data show a temperature overshoot at down-flow (the hot part of the shock)—the temperature is greater than the value at down-flow—[31,57,58], but this characteristic is not present in the NSF equations, as can be seen in Fig. 2.

In addition, we can use the normalized temperature profile defined as

$$T_n(s_A) = \frac{T(s_A) - T_0}{T_1 - T_0}, \tag{31}$$

where T_0 and T_1 are the temperatures at up-flow and down-flow, respectively. The normalized temperature profiles obtained with DSMC are shown in Fig. 3. We notice that the density-temperature separation denoted by $\delta_{T\,\rho}$—defined as the difference in reduced distance between the value at which $\rho_n(0) = 0.5$ ($s_A = 0$) and that at which $T_n(s_A^T) = 0.5$; $\delta_{T\,\rho} = |s_A^T|$—is not very different from the DSMC values as shown in Figs. 3(a) and 3(c). This distance can be seen in Figs. 3(a) and 3(c), and they are consistent between themselves. However, we think it is more important to compare the normalized temperature profiles as shown in Figs. 3(b) and 3(d) that reassure that the temperatures given by the solution to Eqs. (23) are not consistently produced for high Mach numbers, even when the predicted normalized density profiles are.

We end this section by considering two features that are seldom considered in the literature. First, the effect of the initial conditions to solve Eqs. (21), and second, the independence of the predicted normalized density profiles in terms of the reduced variables considered here.

In Figs. 4(a) and 4(c), we show the effect of taking different initial conditions to solve the NSF equations for $\sigma = 0.9$ and $M = 6$ where the critical points are $(1,1/60)$ (up-flow) and $(13/48,2327/11520)$ (down-flow). In Fig. 4(a) the initial condition used is $\mathbf{P}_1 \equiv (13/48 + 10^{-12},2327/11520) \approx (0.2708333333,0.2019965278)$, while in Fig. 4(c) it is equal to $\mathbf{P}_2 \equiv (0.2686783094,0.20)$, the initial value of s (or s_A) is chosen so that the solution at $s = 0$ gives a normalized density profile with value $1/2$ to a certain tolerance, the initial value

TABLE II. Experimental and theoretical values given by the solution to Eqs. (21), for different values of the temperature-viscosity index, of the reduced reciprocal shock thickness (δ_E,δ_T), and the asymmetry of the density profiles for Argon (Q_E,Q_T). Numbers in bold are the present calculations using Eqs. (21); the numbers in parentheses refer to an independent computation with Eqs. (23).

M	σ	$\frac{\lambda_A}{\delta_T}$	$\frac{\lambda_A}{\delta_E}$	Q_T	Q_E
8	0.90	**0.26 (0.26)**	0.24 [65]	**1.26 (1.26)**	1.13 [65]
8	0.86	**0.29 (0.29)**	0.24 [65]	**1.28(1.28)**	1.13 [65]
8	0.81	**0.34 (0.33)**	0.24 [65]	**1.30 (1.30)**	1.13 [65]
8	0.72	0.42 [51]	0.24 [65]	1.4 [51]	1.13 [65]
8	0.72	**0.44 (0.44)**	0.24 [65]	**1.34 (1.35)**	1.13 [65]
6	0.90	**0.30 (0.30)**	0.275 [63]	**1.26 (1.26)**	1.08 [63]
6	0.86	**0.33 (0.34)**	0.275 [63]	**1.27 (1.28)**	1.08 [63]
6	0.81	**0.37 (0.38)**	0.275 [63]	**1.30 (1.30)**	1.08 [63]
6	0.72	**0.46 (0.47)**	0.275 [63]	**1.34 (1.37)**	1.08 [63]
1.55	3.0	**0.08 (0.08)**	0.12 [65]	**0.81 (0.85)**	0.92 [65]
1.55	1.6	**0.13 (0.13)**	0.12 [65]	**1.00 (1.01)**	0.92 [65]
1.55	0.9	**0.17 (0.17)**	0.12 [65]	**1.13 (1.13)**	0.92 [65]
1.55	0.86	**0.17 (0.17)**	0.12 [65]	**1.13 (1.14)**	0.92 [65]
1.55	0.81	**0.17 (0.17)**	0.12 [65]	**1.14 (1.15)**	0.92 [65]
1.55	0.72	**0.18 (0.18)**	0.12 [65]	**1.16 (1.18)**	0.92 [65]
1.2	3.0	**0.053 (0.054)**	0.05 [66]	**0.90(0.96)**	
1.2	0.9	**0.07 (0.07)**	0.05 [66]	**1.06 (1.03)**	
1.2	0.86	**0.07 (0.07)**	0.05 [66]	**1.06(1.04)**	
1.2	0.81	**0.07 (0.07)**	0.05 [66]	**1.06 (1.04)**	
1.2	0.72	0.08 [51]	0.05 [66]	1.07 [35]	
1.2	0.72	**0.07 (0.07)**	0.05 [66]	**1.07(1.04)**	

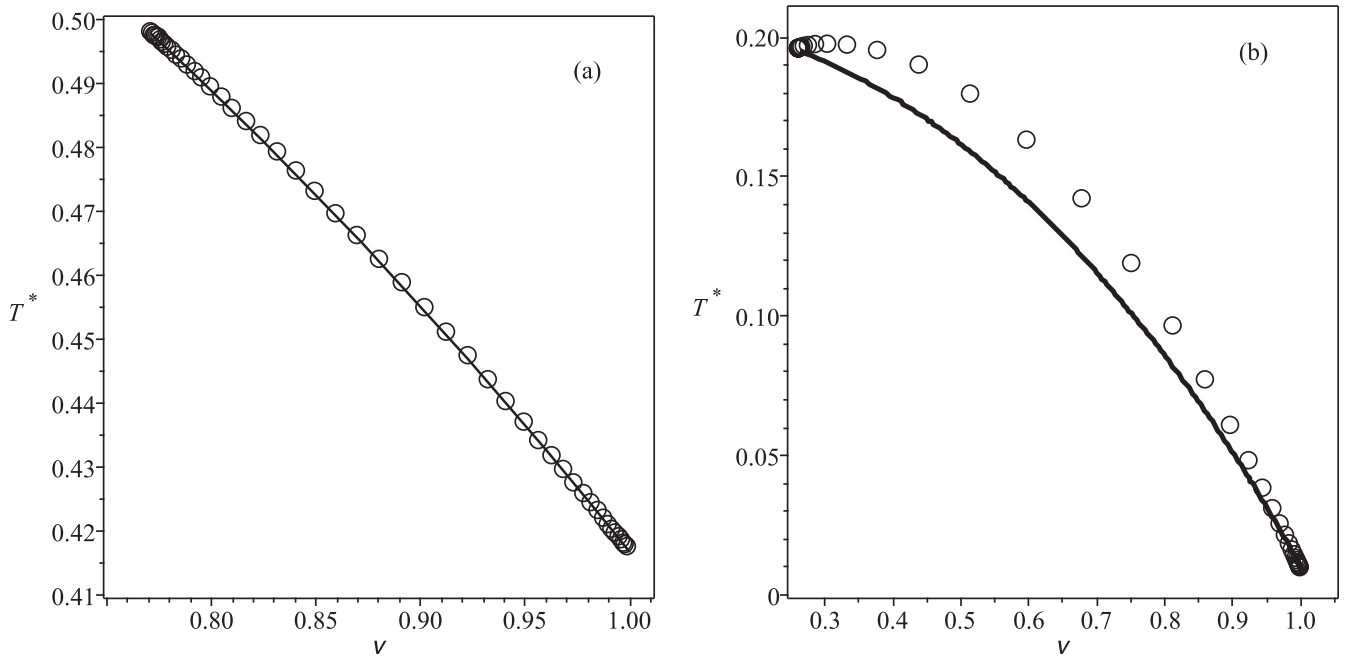

FIG. 2. Orbits (solution curves) for Argon at different Mach numbers. (a) Orbit (solution curve) in the T^*-v plane at $M = 1.2$. Solid line: solution to Eqs. (23); open circles: DSMC for $\sigma = 3$ and $\alpha^{-1} = 0.6015$. (b) Orbit (solution curve) in the T^*-v plane at $M = 8$. Solid line: Solution to Eqs. (23), recall that the orbits are independent of the viscosity; open circles: DSMC with $\sigma = 0.81$ and $\alpha^{-1} = 0.6015$.

of s (or s_A) is different for each initial condition. One would be tempted to say that the initial condition $\mathbf{P}_2$ gives a better agreement with the experiments (specially near down-flow) for Ne, but an important issue here is the asymptotic behavior of the numerical solutions. The solution to the NSF equations generated with the initial condition $\mathbf{P}_2$ does not behave in the way expected for a heteroclinic orbit, meaning that the flat region corresponding to $\rho_n = 1$ should extend to $s_A = \infty$ (or $s \to \infty$). Actually, the solution to the NSF equations using $\mathbf{P}_1$ also has a similar behavior (not shown) but has a flatter plateau.

There are relatively minor discrepancies of our computations for the asymmetry quotient and those reported by other authors; see, for example, the case for $M = 8$ and $\sigma = 0.72$ given in Table II, which can be attributed to the initial conditions used, but to be sure a different approach to calculate the asymmetry quotient was performed. It consists in using the same initial condition for the velocity ($v_i = v_1 + 10^{-10}$) and solving the differential equation for the orbits, which we obtained from Eqs. (23), to get T^* as a function of v, when the normalized density is equal to $1/2$ the value of v can be determined (say v_0) and the corresponding value of T^* (say T_0^*) can be obtained from the solution to the differential equations. Then the differential equations for v and T^*, see Eqs. (23), were solved using the initial condition $v(0) = v_0$ and $T^*(0) = T_0^*$ and from the numerical solution the value of the asymmetry quotient was calculated. The results of the two approaches used to calculate the asymmetry quotient are given in Table II; in most cases, there is fair agreement in the two calculations but differences exist. We think that the differences in the two ways we evaluated the asymmetry quotient together with the values reported in the literature can provide an estimation of the accuracy of the calculations.

One prediction that follows from the NSF equations is that, in terms of the reduced variables used here, the normalized density profiles are independent of the physical system and depend only on the Mach number; this is tested for Krypton and Xenon in Fig. 4(b). It follows that such a prediction is relatively good when compared with the experimental values reported by Steinhilper [64]. The sensitivity of the calculated normalized density profiles with respect the viscosity-temperature index is considered in Figs. 4(b) and 4(d).

IV. CONCLUDING REMARKS

The hydrodynamic model considered in this work (NSF hydrodynamics model) considers the conservation equations given by Eqs. (1), the equations of state given by Eqs. (2), and the Navier-Stokes-Fourier constitutive equations given by Eqs. (3). This leads to solve Eqs. (21) or, equivalently, Eqs. (23). The main conclusion is that the experimental normalized density profiles can be explained with Eqs. (23) when the viscosity-temperature index of the soft sphere model is regarded as an adjustable parameter for Mach numbers ranging from 1.2 to 8; see Fig. 1. The agreement between the experimental reciprocal shock thickness and our hydrodynamic model is also good for the viscosity-temperature index reported in this work. However, concerning the density profile asymmetry, the consistency between experimental data and the NSF soft model as calculated here improve previous studies using Navier-Stokes-Fourier constitutive equations. Figure 1(c) suggests that the viscosity-temperature index can also be taken as an adjustable parameter for the DSMC calculations—the index appears in the definition of the VSS interaction model, see the discussion below Eq. (26)—but the possibility has not been

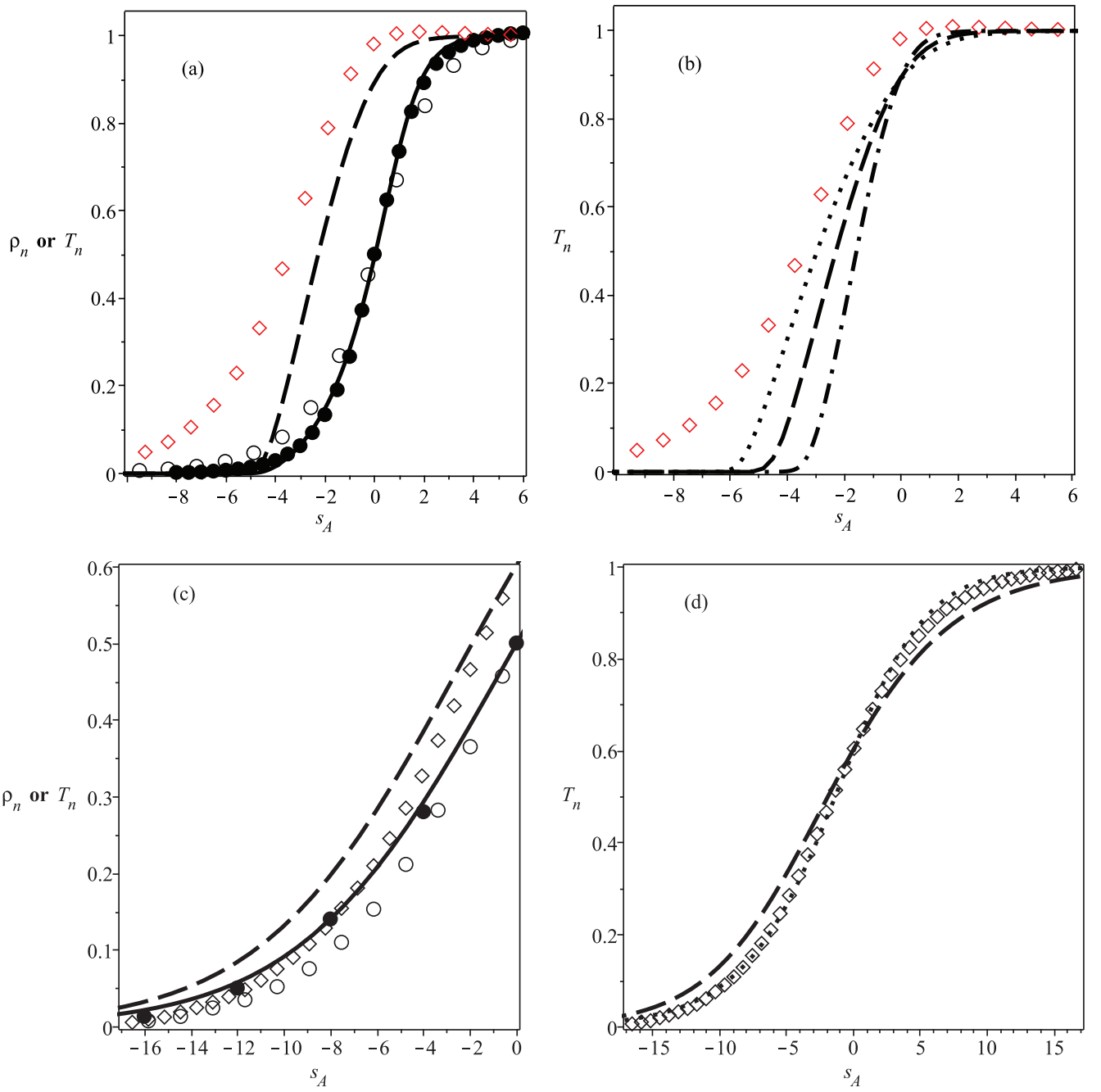

FIG. 3. Normalized density or temperature profiles for Argon versus Alsmeyer's reduced distance, ρ_n or T_n vs s_A. (a)ρ_n and T_n vs s_A for $M = 8$. Experiments [64]: solid circles for ρ_n. DSMC ($\sigma = 0.81$, $\alpha^{-1} = 0.6015$): open circles for ρ_n, diamonds for T_n. Solution to Eqs. (23) for $\sigma = 0.9$: solid line for ρ_n, dashed line for T_n. (b) T_n vs s_A for $M = 8$. DSMC ($\sigma = 0.81$, $\alpha^{-1} = 0.6015$): diamonds. (c) ρ_n and T_n vs s_A for $M = 1.2$. Experiments [66]: solid circles for ρ_n. DSMC ($\sigma = 0.81$, $\alpha^{-1} = 0.6015$): open circles for ρ_n, diamonds for T_n. Solution to Eqs. (23) for $\sigma = 3.0$: solid line for ρ_n, dashed line for T_n. (d) T_n vs s_A for $M = 1.2$. DSMC ($\sigma = 0.81$, $\alpha^{-1} = 0.6015$): diamonds. Solutions to Eqs. (23): dashed line for $\sigma = 3.0$; dotted line for $\sigma = 0$.

explored in this work. Of course, it is not necessary to use the DSMC calculations to fit the experimental normalized profiles using the NSF hydrodynamic model.

The DSMC calculations allow us to perform further comparisons since they include the temperature, so the normalized temperature profiles given by DSMC can be compared with those coming from the NSF hydrodynamic model, as well as the orbits. For Mach numbers near one [$M = 1.2$ in Fig. 3(d)] the viscosity-temperature index that gives better agreement for the normalized temperature profiles ($\sigma = 0$) is different from the one that gives a better agreement for the experimental normalized density profiles ($\sigma = 3.0$). For greater Mach numbers ($M = 8$ in Fig. 3), the temperature profiles predicted by our NSF hydrodynamic model and the DSMC data are very different. This can also be seen in the predicted orbits shown in Fig. 2; we recall that the orbits of

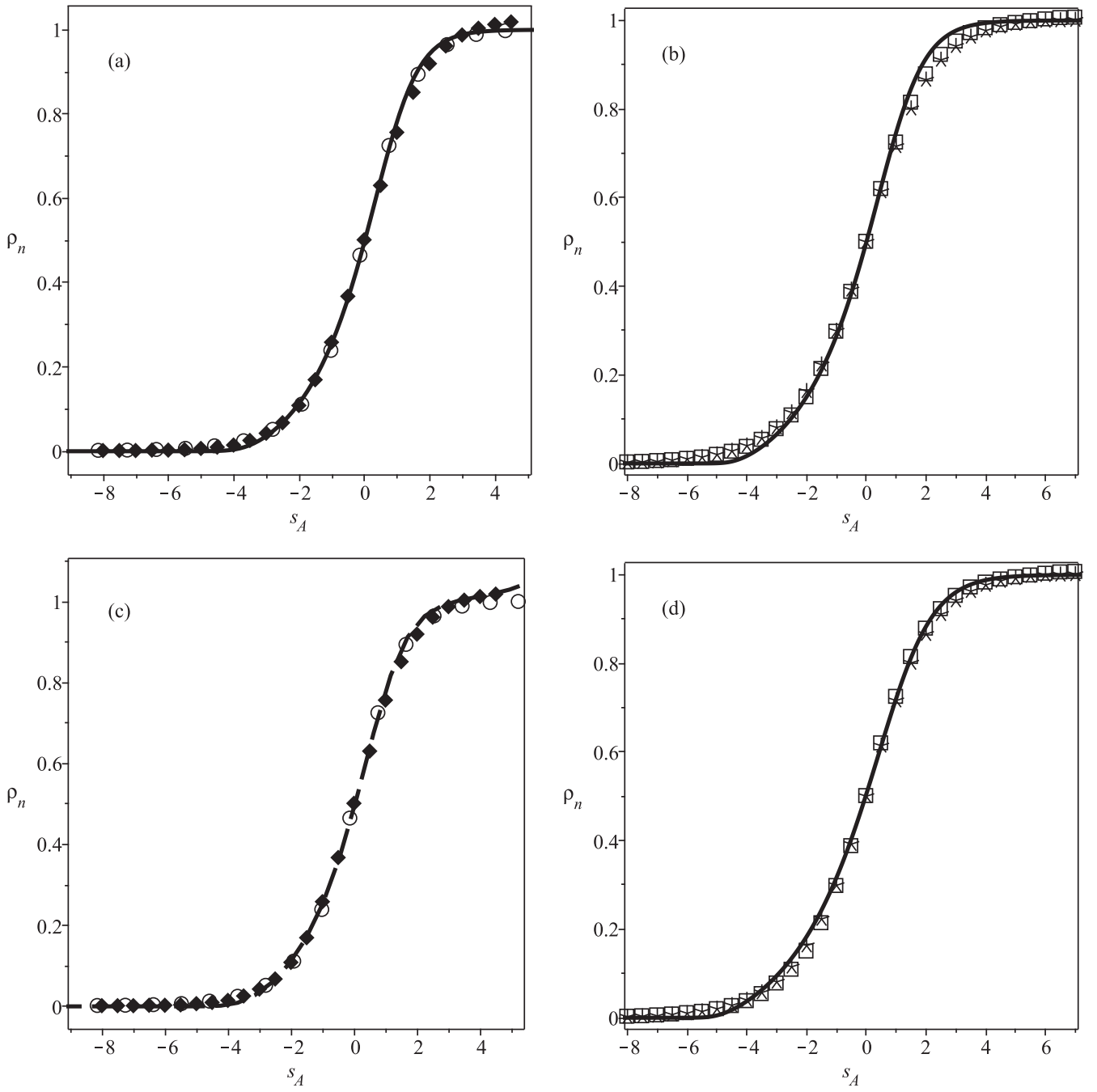

FIG. 4. Normalized density profiles vs the reduced distance, ρ_n vs s_A, for different systems and Mach numbers. (a) $M = 6$. Solid diamonds: Experiments for Neon from Steinhilper [64]; open circles: DSMC for Neon with $\sigma = 0.66$ [57] and $\alpha^{-1} = 1.0$; solid line: Solution to Eqs. (23) for $\sigma = 0.9$ with initial condition $\mathbf{P}_1 = (13/48 + 10^{-12}, 2327/11520)$. (b) $M = 8$. Boxes: experiments for Krypton from Steinhilper [64]; asterisks: experiments for Xenon from Steinhilper [64]; solid line: solution to Eqs. (23) for $\sigma = 0.9$. (c) M = 6. Solid diamonds: experiments for Neon from Steinhilper [64]; open circles: DSMC for Neon with $\sigma = 0.66$ [57] and $\alpha^{-1} = 1.0$; dashed line: solution to Eqs. (23) for $\sigma = 0.9$ with initial condition $\mathbf{P}_2 = (0.2708333333, 0.2019965278)$. (d) $M = 8$. Boxes: Experiments for Krypton from Steinhilper [64]; asterisks: experiments for Xenon from Steinhilper [64]; solid line: solution to Eqs. (23) for $\sigma = 0.95$.

NSF equations are independent of the viscosity-temperature index, but for Mach numbers near one ($M = 1.2$ in Fig. 2) the agreement is satisfactory. The NSF hydrodynamic model considered here fails to give the temperature overshoot near down-flow predicted by DSMC for Mach numbers about 8, see Fig. 2(b), though the lack of experimental data does not allow to decide about such an specific point.

The relevant physical explanation for the better description of the shock-wave problem done here is the enhancement of the transport coefficients when compared to the reported experimental values of the viscosity and thermal conductivity. The results of our NSF hydrodynamical model are good for Mach numbers near 1.5 but deteriorate for Mach numbers about 8, though there is an important improvement for the

normalized density profiles when compared to theories in which such enhancement is not taken into account. The fact that the calculated normalized temperature profiles do not compare well with the simulations for high Mach numbers suggest that there could be a missing physical mechanism that must be taken into account.

Last, it is well known that the description and understanding of the shock-wave structure poses a very big challenge in several aspects, not only in fluid mechanics, kinetic theories, numerical calculations, etc. In this work we have tried to improve the performance of the phenomelogical approach based on the Navier-Stokes-Fourier constitutive equations with a single adjustable parameter. However, it should be desirable to give a physical construction to go deeper even in the phenomenological treatment in this problem. In particular, taking the work done here as a starting point of departure, we can extract some questions to study in the near future. For example, the viscosity-temperature index to describe the shock wave is greater than the one needed to give a good account of the temperature dependence in the viscosity as reported directly from the shear viscosity measurements. We know that the relation between viscosity and the thermal conductivity may not be the same, hence: What kind of relation must be taken? Does the bulk viscosity play a role as some authors have mentioned [21]? Is it possible to give a phenomenological argument to assume a different behavior for such properties? And so on.

[1] L. D. Landau and E. M. Lifshitz, *Fluid Mechanics* (Pergamon Press, Oxford, 1986).
[2] S. Chapman and T. G. Cowling, *The Mathematical Theory of Nonuniform Gases* (Cambridge University Press, Cambridge, 1970).
[3] P. Bhatnagar, P. P. Gross, and M. Krook, Phys. Rev. **94**, 511 (1954).
[4] G. I. Taylor, Proc. R. Soc. London A **84**, 371 (1910).
[5] M. Morduchow and P. A. Libby, J. Aeronaut. Sci. **16**, 674 (1949).
[6] D. Gilbarg and D. Paolucci, J. Ration. Mech. Anal. **2**, 617 (1953).
[7] B. M. Johnson, J. Fluid Mech. **745**, R1 (2014).
[8] D. Burnett, Proc. London Math. Soc. **39**, 385 (1935).
[9] C. Truesdell and R. G. Muncaster, *Fundamentals of Maxwell's Kinetic Theory of a Simple Monatomic Gas* (Academic Press, New York, 1980).
[10] K. A. Fiscko and D. R. Chapman, in *Rarefied Gas Dynamics*, edited by E. P. Muntz, D. P. Weaver, and D. H. Campbell (AIAA, Reston, VA, 1989), pp. 374–395.
[11] E. Salomons and M. Mareschal, Phys. Rev. Lett. **69**, 269 (1992).
[12] X. Zhong, R. W. MacCormack, and D. R. Chapman, AIAA J. **31**, 1036 (1993).
[13] M. Slemrod, J. Stat. Phys. **91**, 285 (1998).
[14] F. J. Uribe, R. M. Velasco, and L. S. García-Colín, Phys. Rev. Lett. **81**, 2044 (1998).
[15] M. S. Shavaliyev, J. Appl. Math. Mech. **63**, 427 (1999).
[16] R. K. Agarwal, K.-Y. Yun, and R. Balakrishnan, Phys. Fluids **13**, 3061 (2001).
[17] T. Ohwada and K. Xu, J. Comput. Phys. **201**, 315 (2004).
[18] L. S. García-Colín, R. M. Velasco, and F. J. Uribe, Phys. Rep. **465**, 149 (2008).
[19] A. V. Bobylev, M. Bisi, M. P. Cassinari, and G. Spiga, Phys. Fluids **23**, 030607 (2011).
[20] S. K. Dadzie, J. Fluid Mech. **716**, R6 (2013).
[21] G. Emanuel, Shock Waves **25**, 11 (2015).
[22] A. V. Bobylev, Philos. Trans. R. Soc. A **376**, 20170227 (2018).
[23] B. L. Holian, M. Mareschal, and R. Ravelo, Phys. Rev. E **83**, 026703 (2011).
[24] H. Grad, Commun. Pure Appl. Math. **5**, 257 (1952).
[25] L. H. Holway, Phys. Fluids **7**, 911 (1964).
[26] D. Jou and D. Pavón, Phys. Rev. A **44**, 6496 (1991).
[27] T. Ruggeri, Phys. Rev. E **47**, 4135 (1993).
[28] W. Weiss, Phys. Rev. E **52**, R5760(R) (1995).
[29] M. AlGhoul and B. Eu, Phys. Rev. E **56**, 2981 (1997).
[30] D. Baganoff, Phys. Fluids **14**, 3403 (2002).
[31] M. Torrilhon and H. Struchtrup, J. Fluid Mech. **513**, 171 (2004).
[32] X.-J. Gu and D. R. Emerson, J. Fluid Mech. **636**, 177 (2009).
[33] Z. Cai, R. Li, and Y. Wang, Commun. Comput. Phys. **11**, 1415 (2012).
[34] M. Torrilhon, Annu. Rev. Fluid Mech. **48**, 429 (2016).
[35] F. J. Uribe, Phys. Rev. E **93**, 033110 (2016).
[36] M. Y. Timokhin, H. Struchtrup, A. A. Kokhanchik, and Y. A. Bondar, Phys. Fluids **29**, 037105 (2017).
[37] I. Karlin, Philos. Trans. R. Soc. A **376**, 20170230 (2018).
[38] H. M. Mott–Smith, Phys. Rev. **82**, 885 (1951).
[39] A. G. Bashkirov and A. V. Orlov, Phys. Rev. E **53**, R17(R) (1996).
[40] Y. Ohr, Phys. Fluids **13**, 2105 (2001).
[41] M. A. Solovchuk and T. W. H. Sheu, Phys. Rev. E **81**, 056314 (2010).
[42] E. A. Mason and E. W. McDaniel, *Transport Properties of Ions in Gases* (Wiley, New York, 1988).
[43] B. L. Holian, C. W. Patterson, M. Mareschal, and E. Salomons, Phys. Rev. E **47**, R24(R) (1993).
[44] F. J. Uribe, R. M. Velasco, and L. S. García-Colín, Phys. Rev. E **58**, 3209 (1998).
[45] Y.-G. He, X.-Z. Tang, and Y.-K. Pu, Phys. Rev. E **78**, 017301 (2008).
[46] K. Xu, X. He, and C. Cai, J. Comput. Phys. **227**, 6779 (2008).
[47] W. G. Hoover and C. G. Hoover, *Time Reversibility, Computer Simulation, Algorithms, Chaos* (World Scientific, Singapore, 2012).
[48] F. J. Uribe, W. G. Hoover, and C. G. Hoover, Comput. Methods Sci. Technol. **18**, 5 (2013).
[49] D. Madjarevic and S. Simić, Europhys. Lett. **102**, 44002 (2013).
[50] H. Brenner, Physica A **349**, 60 (2005).
[51] C. J. Greenshields and J. M. Reese, J. Fluid Mech. **580**, 407 (2007).
[52] H. Brenner, Physica A **388**, 3391 (2009).
[53] F. J. Uribe, in *Coping with Complexity: Model Reduction and Data Analysis*, edited by A. N. Gorban and D. Roose (Springer-Verlag, Berlin, 2011), pp. 207–229.
[54] L. G. Margolin, Philos. Trans. R. Soc. A **367**, 2861 (2009).

[55] L. G. Margolin, Philos. Trans. R. Soc. A **376**, 20170235 (2018).
[56] P. Glansdorff, Phys. Fluids **5**, 371 (1962).
[57] G. A. Bird, *Molecular Gas Dynamics and the Direct Simulation of Gas Flows* (Oxford-Clarendon, New York, 1994).
[58] G. A. Bird, *The DSMC Method (version 1.2)* (G. A. Bird, Lexington, 2013).
[59] W. G. Hoover, Phys. Rev. Lett. **42**, 1531 (1979).
[60] Y. Qian, D. Dhumieres, and P. Lallemand, Europhys. Lett. **17**, 479 (1992).
[61] J. M. Buick, C. L. Buckley, C. A. Greated, and J. Gilbert, J. Phys. A: Math. Gen. **33**, 3917 (2000).
[62] S. Succi, I. V. Karlin, and H. Chen, Rev. Mod. Phys. **74**, 1203 (2002).
[63] B. S. Schmidt, J. Fluid Mech. **39**, 361 (1969).
[64] E. A. Steinhilper, Electron beam measurements of the shock wave structure, Ph.D. thesis, California Institute of Technology, USA, 1971.
[65] H. Alsmeyer, J. Fluid Mech. **74**, 497 (1976).
[66] W. Garen, R. Synofzik, and G. Wortberg, in *Rarefied Gas Dynamics*, edited by J. L. Potter (AIAA, Reston, VA, 1977), Vol. 1426.
[67] R. Caflisch and B. Nicolaenko, Commun. Math. Phys. **86**, 161 (1982).
[68] S. Takata, K. Aoki, and C. Cercignani, Phys. Fluids **12**, 2116 (2000).
[69] T. G. Elizarova, A. A. Khokhlov, and S. Montero, Phys. Fluids **19**, 068102 (2007).
[70] G. C. Pham-van-Diep, D. A. Erwin, and E. Muntz, J. Fluid Mech. **232**, 403 (1991).